Jim Thomson, Phil Bush, Viviana Castillo Con...
Davis, Alex de Klerk, Emily Iseley, Edwin James Rainvi...
2023): Development and testing of microSWIFT expendabl...

Submit your article to this journal

View related articles

View CrossMark data

RESEARCH ARTICLE

# Development and testing of microSWIFT expendable wave buoys

Jim Thomson ⓘ, Phil Bush, Viviana Castillo Contreras, Nate Clemett, Jacob Davis ⓘ, Alex de Klerk, Emily Iseley, Edwin James Rainville ⓘ, Brenton Salmi and Joe Talbert

Applied Physics Laboratory, University of Washington, Seattle WA, USA

**ABSTRACT**

Expendable microSWIFT buoys have been developed and tested for measuring ocean surface waves. Wave spectra are calculated via onboard processing of GPS velocities sampled at 5 Hz, and wave spectra are delivered to a shore-side server via Iridium modem once per hour. The microSWIFTs support additional sensor payloads, in particular seawater conductivity and temperature. The buoys have a non-traditional, cylindrical shape that is required for deployment via the dropsonde tube of research aircraft. Multiple versions have been developed and tested, with design considerations that include: buoy hydrodynamics, sensor noise, algorithm tuning, processor power, and ease of deployment. Field testing in a range of conditions, including near sea ice and in a hurricane, has validated the design.

## 1. Introduction

The modern era of ocean wave measurements is defined by an expansion in operational remote sensing (e.g. satellite altimeters, lidar scanners) and by a flood of inexpensive wave buoys (e.g. Spotter buoys, openMet buoys). Amidst the plethora of miniature wave buoys, one can and should ask if another wave buoy is needed. The answer is that specific projects often require unique features or sampling modes not available in existing buoy designs. Our development of microSWIFT buoys has been motivated by several specific projects needs, including: access to raw data for phase resolved models, high sampling rates for breaker detection, robustness in sea ice, aerial deployment from the dropsonde tube of research aircraft, and inclusion of additional sensors as modular payloads.

Collins et al. (2024) provides a thorough review of wave buoy measurements and an inter-calibration effort for several miniature wave buoys. Much of this activity traces directly back to Herbers et al. (2012), who demonstrated the utility of Global Positioning System (GPS) Doppler velocities as the raw motion data for wave spectral analysis. This was a departure from the classic pitch-roll-heave motion data (Kuik, Van Vledder, and Holthuijsen 1988), and thus the use of GPS data helped launch a new generation of wave buoys. The SWIFT buoys (Thomson 2012) immediately adopted the GPS approach, as did many other buoys and platforms (Raghukumar et al. 2019; Thomson et al. 2018). Other modern buoys have used newly available, low-cost Inertial Motion Unit (IMU)

sensors (Feddersen et al. 2024; Rabault et al. 2020, 2022). The development of microSWIFT buoys has explored both GPS and IMU approaches, as part of a larger effort to miniaturize the original SWIFT design and end up with something compact and expendable.

The goal of this paper is to describe the development and testing of microSWIFT buoys, with particular attention to lessons learned that have steadily improved the quality of the wave data and the usability. Section 2 describes the design of the buoys, Section 3 describes the algorithms, Section 4 describes testing the buoys, and Section 5 summarizes the deployments to-date.

## 2. Buoy design

There have been three versions of microSWIFT buoys to date, each with a few variations. The first beta version was a simple proof-of-concept. Subsequent versions have evolved to address weaknesses identified during testing and to address new mission requirements associated with new research projects. Figure 1 shows the different physical designs, and Table 1 summaries the specifications. The choice of a cylindrical buoy shape throughout all versions, rather than the more common spherical buoy shape, is driven by a requirement for aerial deployments using the A-sized tube (nominal 5-inch diameter) for dropsondes from research aircraft, such as the NOAA *P*-3 Hurricane Hunter or Twin Otter.
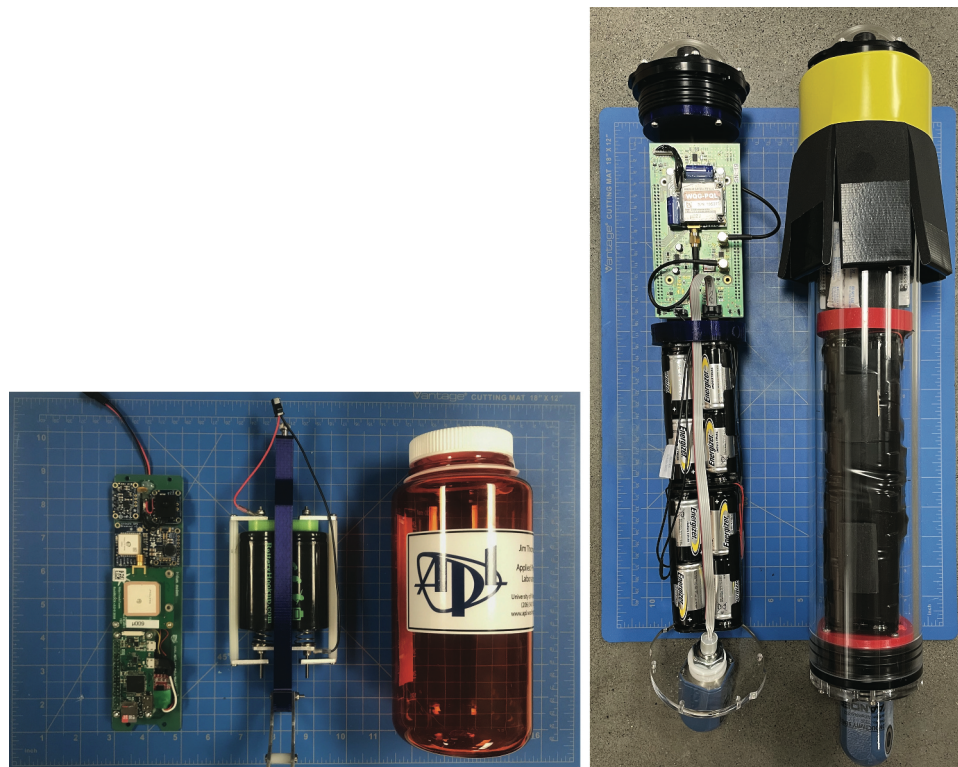
**Figure 1.** microSWIFT versions. Left: v1 in a 1-L Naglene bottle housing. Right: v2 in a 2-L housing (also used in a variation of v1) with an octopus foam collar. The 2-L version has an optional conductivity-temperature (CT) sensor at the bottom of the housing.

**Table 1.** microSWIFT versions.

| Version | Processor | Endurance | Housing | Code base | Tracking/Telemetry | Unit Cost |
|---------|-----------|-----------|---------|-----------|--------------------|-----------|
| beta | none | 1 day | 1-L Naglene | none | Dog collar/none | $250 |
| v1 | RaspberryPi-0 | 2 days | 1-L Naglene | Python | Iridium | $500 |
| v1 | RaspberryPi-0 | 5 days | 2-L Blue Robotics | Python | Iridium | $600 |
| v2 | STM | 30 days | 2-L Blue Robotics | C | Iridium | $900* |

*cost is increased by $2,000 with optional CT sensor.

## 2.1. microSWIFT v-beta

The beta version of the microSWIFT buoy was simply a 1-Liter, Naglene-brand water bottle with two commercial, off-the-shelf components: a GPS logger (Qstarz) and a dog-tracking collar (Garmin Astro). These were first deployed in 2014 to measure the wakes of Washington State Ferries in Rich Passage (Perfect et al. 2015), and later used for the DUNEX pilot in 2019. The endurance was approximately one day, and the system had no onboard processing or telemetry. The buoys had to be recovered (based on tracking with the dog collars) and the raw GPS data offloaded for post-processing.

## 2.2. microSWIFT v1 (1-L and 2-L)

The first production version of the microSWIFT buoy still uses the 1-Liter Naglene bottle as the housing and upgrades the electronics to a RaspberryPi-0 processor on a custom Printed Circuit Board (PCB). This enables integration of a GPS receiver and IMU, with onboard processing and telemetry of results via Iridium modem. The RPi processor is an excellent choice for rapid, collaborative software development. A set of Python codes, managed in a public GitHub repo (https://github.com/SASlabgroup/microSWIFT) controls all aspects of data logging, processing, and telemetry. The RPi is also an excellent choice for short-deployments, because the WiFi connectivity can be used to automate the offload and organization of raw data from a large number of buoys (once recovered and in range of the network). This was helpful during the DUNEX main experiment, when up to 50 buoys were deployed on daily missions and post-processing raw data was essential (Rainville et al. 2023).

The RPi is a less ideal choice in terms of power usage. The v1 buoys use approximately 200 mW on-average, and most of this is the RPi itself (as opposed to the GPS, IMU, or Iridium modem). For the 1-L Naglene bottle housing with two D-cell rechargeable batteries, the maximum mission life is two days. A 2-L housing, based on Blue Robotics 3-inch inner diameter pressure

cases, provides space for 16 C-cell batteries and extends mission life to five days. This has been essential for successful deployments during the first year of the NOPP Hurricane Coastal Impacts (NHCI) program (see Section 5). The 2-L housing also includes a dedicated GPS antenna that improves the quality of the GPS velocities.

### 2.3. microSWIFT v2

The second production version of the microSWIFT replaces the RaspberryPi with a low-power microprocessor (STM32). This increases the endurance to approximately 30 days with the same 2-L housing and 16 Alkaline C-cell batteries. The increased endurance enables persistent observing that can capture events, especially in the western Arctic and in the tropical Atlantic pathway for hurricanes (see Section 5). The switch to a microprocessor includes a switch to C as the codebase and more specialized/intensive software development. Compared with the numerous Python libraries available for the RPi on v1, much of the C software for v2 had to be developed from scratch.

The v2 microSWIFT upgrades the GPS receiver to a multi-constellation GNSS unit (UBlox M10) which tracks up to 32 satellites at a time, compared with 16 GPS satellites tracked by most consumer grade GPS receivers. The additional satellites tracked are from the GALILEO, GLONASS, and BEIDOU constellations in orbit. The additional satellites improve the accuracy of the velocity components used as inputs to the onboard wave processing (Section 3), especially the vertical component of velocity. Errors in velocity components are expected to be $< 0.05$ m/s.

The v2 microSWIFT has a new PCB to integrate the microprocessor, GNSS receiver, and Iridium modem. Provisions for an IMU exist, though it is not included in the present onboard processing (see Section 3). There is also magnetic power switch, such that it can be turned on without opening the pressure case or the air-deployment rigging. The v2 microSWIFT also includes a conductivity and temperature (CT) sensor (Aanderaa 4319) at the bottom of the 2-L hull for determination of sea surface salinity and sea surface temperature (approximate measurement depth 0.2 m). This continues a general modular sensor approach used in the original full-scale SWIFTs, which have supported the same model CT for years (along with acoustic Doppler profilers, meteorological sensors, cameras, fluorometers, etc).

### 3. Onboard data processing

This section describes the microSWIFT onboard processing of GPS data to produce the standard ocean wave spectral and bulk metrics. Testing of the v1

microSWIFT included several iterations using the IMU data to produce similar metrics, as done on some other mini buoys (Feddersen et al. 2024; Rabault et al. 2020, 2022). Although post-processing the IMU data produced excellent results from the DUNEX project (Rainville et al. 2023), it has not been adopted as the standard for onboard processing. Two key problems have prevented the use of IMU data for onboard processing: 1) the correction from the body reference frame to the earth reference frame, and 2) the introduction of spurious energy at low frequencies when integrating motion data to estimate position. Both of these problems can be solved with sufficient computational power, filtering, and calibration.

Rather than implement IMU sensor-fusion algorithms onboard or rely on black-box state estimates, we have chosen to use the GPS velocities exclusively in the onboard processing. These velocities are agnostic to buoy orientation and already in an earth reference frame, with orthogonal north-east-down components $(v, u, w)$. This approach is particularly well suited to non-spherical shapes that may not follow surface slopes. The processing uses the frequency spectra $S(f)$ of the components to estimate the scalar energy spectra,

$$E(f) = \frac{S_{uu}(f) + S_{vv}(f)}{(2\pi f)^2} \qquad (1)$$

and the standard directional moments,

$$a_1(f) = \frac{\text{Im}(S_{uw})}{\sqrt{(S_{uu}(f) + S_{vv}(f))S_{ww}(f)}},$$
$$b_1(f) = \frac{\text{Im}(S_{vw})}{\sqrt{(S_{uu}(f) + S_{vv}(f))S_{ww}(f)}}, \qquad (2)$$

$$a_2(f) = \frac{S_{uu}(f) - S_{vv}(f)}{S_{uu}(f) + S_{vv}(f)}, \qquad b_2(f) = \frac{2\text{Re}(S_{uv}(f))}{S_{uu}(f) + S_{vv}(f)} \qquad (3)$$

For more information and diagrams interpreting the directional moments $a_1, b_1, a_2, b_2$, see the appendix of Thomson et al. (2018). The use of horizontal velocities in Eq. 1 assumes circular orbits in deep water. This assumption could be relaxed by the use of vertical velocities, which have the same $f^{-2}$ relation to sea surface spectra in any water depth. However, the vertical velocities tend to have higher levels of noise, and thus are not preferred. The assumption of circular orbits is evaluated with another spectral quantity that is calculated onboard, which is the ratio of vertical to horizontal motion known as the check factor

$$check\,(f) = \frac{S_{ww}(f)}{S_{uu}(f) + S_{vv}(f)}. \qquad (4)$$

This should be equal to one in deep water. Note that energy spectra $E(f)$ derived from horizontal velocities with a deep-water assumption can be

adjusted for intermediate water depth (if known) by using the linear dispersion relation.

The onboard processing code was developed in Matlab and the source is included the public SWIFTcodes GitHub repository (https://github.com/SASlabgroup/SWIFT-codes/waves/NEDwaves.m). For the v1 microSWIFTs, this was translated to Python. For the v2 microSWIFTs, this was built as a C static library using the Matlab Coder application. Building the C library required some changes to improve memory management, which is not optimized in the Matlab code conversion.

Each 30-minute burst of raw GPS data is processed in windows of 256 s each, with 75% overlap. Prior to an FFT, each window is prepared with a high-pass RC filter to remove drift from the velocities and a variance-preserving cosine taper to remove edge effects. The RC filter is the same as Thomson et al. (2018), where the time constant is set as $4 \times 2\pi \approx 25$ seconds as the longest period retained in the raw time series data. The resulting ensemble spectra have 16 degrees of freedom (from 8 independent windows). This is then increased to 48 degrees of freedom by merging every three neighboring frequency bands. The frequency-band merging also reduces the total size of the final spectrum for telemetry.

Standard bulk parameters are calculated onboard, including significant wave height $H_s = 4\sqrt{\sum E(f)df}$, peak wave period $T_p$, and peak wave direction $D_p$. Other parameters are readily calculated from the onboard spectra, including the energy-weighted centroid period $T_e$ and the mean square slope $mss$.

### 3.1. Telemetry

A key feature of any expendable system is the telemetry of data products, since the raw data will not be recovered. The microSWIFTs use an Iridium Short Burst Data (SBD) modem (model 9603B). The processed wave spectra meta data are assembled onboard as byte arrays and sent in a single binary SBD packet (limit: 340 bytes). This uses half-float precision values to be able to fit all five spectra moments. The custom formatting of this binary packet is readable in Python (https://github.com/SASlabgroup/microSWIFTtelemetry/blob/main/microSWIFTtelemetry/sbd/read_sbd.py) or Matlab (https://github.com/SASlabgroup/SWIFT-codes/blob/master/GeneralTools/readSWIFT_SBD.m).

A shore-side server at APL-UW receives these SBD packets as e-mails and parses them with a Python script. The script populates a database hosted on the server, which is then accessed with an API (Application Protocol Interface). The API is a public interface, which queries the server by building urls for specific buoys, data formats, and times. The API can be queried in a variety of automated modes (curl, wget, etc), and there no difference between the public API and the access of internal APL-UW users. A Python package (https://github.com/SASlabgroup/microSWIFTtelemetry) and a Matlab function (https://github.com/SASlabgroup/SWIFT-codes/blob/master/GeneralTools/pullSWIFTtelemetry.m) are available to work directly with the API. There also is a simple user interface at the data tab of www.apl.uw.edu/swift for accessing data directly via a web browser. A live map showing buoys and data on a rolling three-hour window is also available.

## 4. Initial buoy testing

Prior to field deployments, the buoys are tested to determine: 1) the sensor noise using static tests, 2) the hydrodynamic response using free decay oscillations in a tank, and 3) the motion signals on a rotary test stand. In additions, a series of aerial deployment tests determined the rigging required for the buoys to survive aircraft deployments.

### 4.1. Static noise

The first test for each microSWIFT version is to record a burst of raw data without motion and evaluate the sensor noise. Quantification of sensor noise is particularly important for wave buoys intended for deployment in ice, because even modest noise levels can affect the spectral energy ratios used to calculate wave attenuation by sea ice (Thomson et al. 2021). The static test can be done as part of a bench test, but only if the bench location has sufficient GPS signal. A typical burst of raw data is 2048 seconds long and sampled at 4 Hz. The onboard processing of this data produces an empirical noise spectrum, along with an effective noise height $H_n$. This is only a proxy for uncertainty in the operational wave results, as the sensor noise and buoy dynamics in a given sea state might differ from the static tests. Still, it is a useful check-point in the development process.

Figure 2 shows the noise spectra $E_n(f)$ from both v1 and v2 buoys. The spectra have an expected $f^{-2}$ shape, which results from white noise ($f^0$) in velocity that is converted to elevation (equation 1). These spectra can be integrated to obtain an equivalent noise level in significant wave height, which is generally less than 0.1 m. The v2 buoys have a higher (worse) noise floor, and work is ongoing to reduce this noise. A parallel approach is to remove the noise by simple subtraction of the empirically determined static noise spectrum $E_n(f)$ from each observed wave spectrum $E(f)$, assuming that the noise is
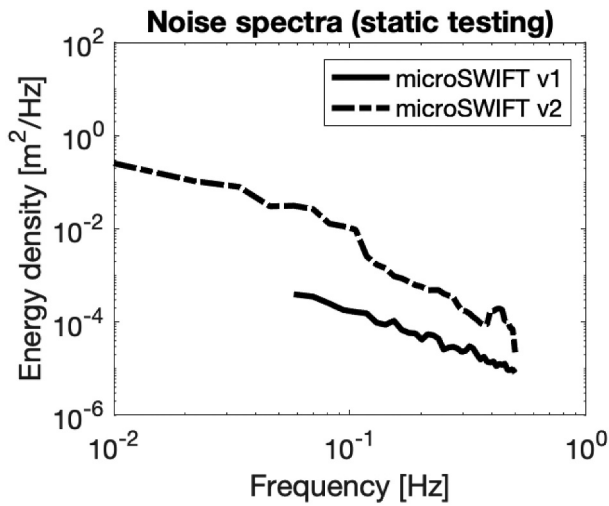
**Figure 2.** Energy spectra from static noise testing of buoys.

uncorrelated from the signal (see Thomson et al. (2021) for discussion of noise super-position). This is promising, though not yet implemented in the operational version of the onboard software.

The increased noise likely is related to the different GPS (or rather, GNSS) receivers, though it could also be the antennas. MicroSWIFT v1 uses a GlobalTop receiver (model FGPMMOPA6H) and an active patch antenna. MicroSWIFT v2 uses a UBlox receiver (model MAX-M10S) and a passive cylindrical antenna, which is shared with the Iridium modem. Although the UBlox is nominally a higher-quality sensor, the noise in the velocity measurements is clearly higher. One possibility is multi-pathing of the GNSS signal caused by the metal ring of the buoy end-cap. However, removing the end-cap during static testing (on land) does not reduce the noise. It is possible that the addition of a grounding plane would help the antenna performance; we plan to try this in a future version. Though the noise is clearly worse for v2, it is still a relatively small effect on significant wave height ($\sim$0.1 m).

### 4.2. Free decay oscillations

The heave response of any floating body can be described as a mass-spring-damper oscillation, which then determines the natural frequency $f_n$ at which the body will bob,

$$f_n = \frac{1}{2\pi} \sqrt{\frac{\rho_w g V}{ML}}. \qquad (5)$$

The buoyancy force is determined by the density of the water $\rho_w$, gravity $g$, and the displaced volume $V$. The mass $M$ and vertical length (draft) $L$ control the inertia. For a spar, the ratio $V/L$ simplifies to $\pi r^2$, and the resulting $f_n$ does not depend on the draft of the buoy. The denominator often includes a term for added mass in addition to the actual mass. This is the water surrounding the buoy that is accelerated with the buoy, and it is usually characterized with an added mass coefficient multiplied by the displaced volume of water. For small objects the added mass adjustment is often negligible. The physical heave added mass of a spar, $A_{\text{heave}} = \frac{2}{3}\pi\rho_w r^3$, for the 2-L hull with radius $r = 4.45$ cm is 0.2 kg, is about 5% of the buoy's mass.

For a wave buoy, the ideal design is a natural frequency that is above the energetic frequencies of ocean waves (nominally $0.05 < f < 0.5$ Hz), such that the buoy has an stiff response to the wave motion. Prior work has shown reduction in buoy response with increasing buoy mass when the natural frequency decreases enough to fall within the wave bands (Thomson et al. 2015). The 1-L microSWIFT has $f_n = 2.00$ Hz and the 2-L microSWIFT has $f_n = 0.75$ Hz. Both meet the nominal requirement for $f_n$ to be greater than the wave frequencies of interest, but that alone does not guarantee buoy performance. The mass, geometry, and theoretical natural frequency of each version are in Table 2. The 2 L designation is a clear misnomer, relative to displaced volume of the buoy, but we retain the name here for legacy reasons and continuity of design documents.

A more comprehensive approach to buoy response is to determine a frequency-dependent Response Amplitude Operator (RAO) for the buoy, based on the response to known forcing. This is rarely uniform in frequency. Instead, it has a resonant peak at the natural frequency (equation 5) and increasing damping away from this frequency. The damping is generally far more severe for $f > f_n$, hence the requirement for $f_n$ to be greater than the wave frequencies of interest. A simple test of both the natural frequency and the RAO is a free decay oscillation, in which the buoy is submerged completely (or dropped) and then allowed to respond without additional forcing. Figure 3 shows the free decay of a 2-L buoy, in which the empirical $f_n \sim 0.77$ Hz confirms the calculated $f_n \sim 0.75$ Hz calculated and shows the damping at frequencies above and below $f_n$.

For the v1-2 L version, damping of resonance at $f_n$ is achieved with a flotation collar that has six

**Table 2.** microSWIFT mass and geometry.

| Version | Orientation | Mass | Length | Diameter | Displaced volume | Natural frequency |
|---------|-------------|------|--------|----------|------------------|-------------------|
| v1-1L | horizontal | 0.9 Kg | 21.4 cm | 9.2 cm | 1.4 L | 2.00 Hz* |
| v1-2L | vertical | 2.8 Kg | 48.3 cm | 8.9 cm | 3.0 L | 0.75 Hz |
| v2-2L | vertical | 2.9 Kg | 51.0 cm | 8.9 cm | 3.2 L | 0.74 Hz |

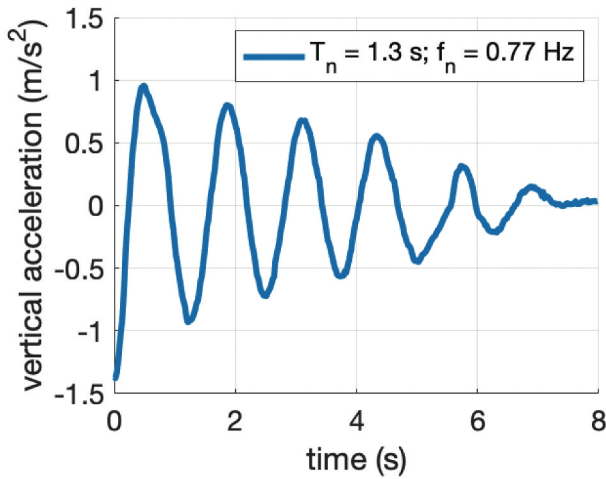*In a vertical configuration, the 1L microSWIFT would have $f_n = 1.38$ Hz.

**Figure 3.** Time series of heave response during free decay test of 2-L buoy.



**Figure 4.** Energy spectra rotary test stand operating at approximate 10 second period ($f \approx 10^{-1}$ Hz).

independent flaps we call the octopus collar[1] The octopus collar uses strips of closed-cell foam that are 2 inches wide and 0.25 inches thick. The six strips are placed lengthwise along the upper hull, then the tops of all strips taped in circumference (see yellow tape banded around the hull in Figure 1). The tape covers and holds the first 2 inches against the hull; a remaining 4 inches of each strip are left to move as independent flaps. The effective waterline is just below the yellow tape, such that the foam flaps are slightly submerged. The flexible response of the flaps damps heave motions, helping keep the dome end-cap and antenna above the surface.

There is also a natural frequency for the tilting (pitch and roll changes) of any buoy. The octopus collar helps damp these motions too, such the buoy remains mostly upright in the water. Deviations from vertical are ignored in onboard data processing because the GPS velocity method is agnostic to buoy orientation. It is simply the lateral translation that matters for $u, v$. The pitch and roll do not affect this, so long as the antenna is close to the center of rotation (Thomson et al. (2018) provide a first-order correction for antennas above the axis of rotation, which is generally small if < 1 m.). An IMU-based approach would be much more sensitive to pitch and roll changes, and corrections from the body reference frame to the earth reference frame would be required (Rainville et al. 2023).

### 4.3. Rotary test stand

Prior to testing in real ocean waves, the fidelity of wave motion quantification can be evaluated with a rotary test stand that simulates orbital wave motion of known amplitude and period. We built a simple version using
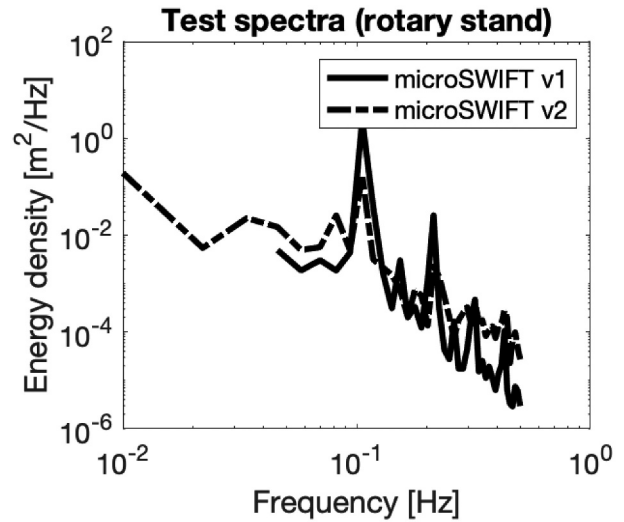
a DC motor, belt-drive, and bicycle mechanic stand. This was used to test both v1 and v2 buoys at amplitudes of 0.5 m ($H = 1$ m) and periods 4 and 10 seconds. For onboard GPS processing, testing indoors produced inferior results even when using a GPS repeater from the roof of the building. Another problem with the rotary test stand is the presence of harmonics in the spectral results, which are presumably from a mechanical instability in the test stand.

Figure 4 shows the results of testing on the rotary stand. Both the v1 and v2 buoys show a clear peak at the driven frequency $f = 0.1$ Hz, as well as a harmonic in the stand around $f = 0.2$ Hz. The background levels in Figure 4 are consistent with the static noise testing in Figure 2.

### 4.4. Air-drop tests

A series of air-drop tests have refined the approach to aerial deployment of the microSWIFTs. The initial tests were simply drops from static platforms less than 50 ft in height (i.e. the upper deck of research vessels and coastal piers) to confirm the electronics and hull were robust. Testing then progressed to dropping from the open door of helicopters (approx. 100 ft height), with the addition of small nylon drogues (24 inch-diameter parachutes). Next, the buoys were packaged in cardboard tubes, with drogues stuffed in the top, for deployment from the A-sized dropsonde tubes of Twin Otter and *P*-3 research aircraft. This was first tested Sept 2021 from a NOAA Twin Otter, then retested in May 2022 from the open-door of a sky-diving plane, then tested in July 2022 with the tube of a *P*-3 operated by the NRL (Navy Research Laboratory) VXS-1 squadron. Operational deployments from the NRL *P*-3 followed in Sept 2022 ahead of Hurricane Ian's landfall on the Gulf coast of Florida. The survival rate from a total of 64 drops conducted to-date is 90%. Success is

---

[1]An octopus technically has six arms and two legs, so this name is not as inaccurate as it might at first seem..
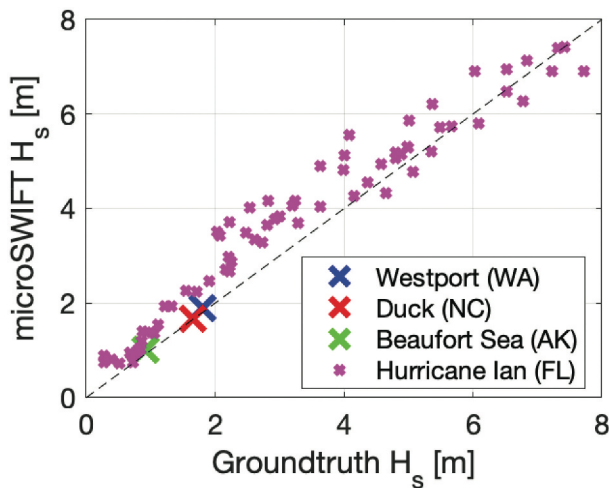
**Figure 5.** Comparison of significant wave heights during field deployments.

generally associated with lower airspeeds ($100 - 130$ knots) and altitudes ($300 - 1000$ feet). Testing is ongoing, especially at the higher air-speeds ($>200$ knots) and altitudes ($10,000$ ft) required for NOAA *P-3* Hurricane Hunter missions.

The established rigging method is to encase the microSWIFT in a cardboard tube, which is split lengthwise and then bound around the microSWIFT with dissolving tape. The tape dissolves rapidly once the buoy hits the water, and the two halves of the cardboard separate to release the buoy to float freely. The bottom of the cardboard tube has several discs of cardboard that act as a crumple zone at the moment of impact with the water. The top of the cardboard tube has the aerial drogue stuffed inside, and a small tail of webbing protruding. The webbing flutters and pulls the drogue from the tube once released from the aircraft. This provides an important delay in the drogue deployment, and thereby insures both safe separation from the aircraft and reduced load on the drogue. The drogue provides only a modest reduction in the fall velocity of the buoy; it is not truly a parachute, but it does help the buoy maintain orientation in air. The drogue is not directly connected to the buoy, rather it is connect to the cardboard using a webbing bridle that threads through each half and below the

buoy. Thus, it also washes free of the buoy upon entering the water.

## 5. Buoy deployments

A series of field deployments, summarized in Table 3, have validated and improved the microSWIFTs. These deployments span routine coastal measurements to extremes (Arctic, hurricanes). Figure 5 compares the microSWIFT significant wave heights $H_s$ during each test with some form of ground truth or other independent estimate of $H_s$. The 2021 tests were all short in duration and limited in $H_s$ range, compared with the 2022 deployment during Hurricane Ian. The Ian deployments, however, suffer from a lack of truly collocated ground truth measurements. The scatter in the collocated testing from 2021 is within the $\pm 0.1$ m error in $H_s$ expected from the static noise testing. The scatter in the Ian 2022 dataset is larger, most likely because the Spotter buoy used for groundtruth was 50–100 km away from the microSWIFT.

Spectral comparisons and details for each test are in the subsections that follow. The short-duration tests from 2021 are presented together in Figure 6 and include results from onboard processing of the IMU data. This was discontinued in later tests, because sufficient filtering of the raw IMU data was not achieved onboard (because of limited computing power). The early tests do not include directional moments ($a_1, b_1, a_2, b_2$), because of a software bug invalidated most the results. These issues were addressed prior to the Hurricane Ian deployments, and thus we focus on the Ian results as a more comprehensive evaluation of the microSWIFTs (including the directional moments).

### 5.1. Westport (Washington State, USA)

Brief test deployments were conducted offshore of Westport and Grays Harbor, Washington State (USA), where a Datawell waverider is maintained as CDIP station 036. There are strong tidal currents at the mouth of Grays Harbor, and adjusting for the Doppler shift between the moored Waverider and the drifting microSWIFTs is important. Testing occurred for a few hours in July 2021 with several

**Table 3.** microSWIFT deployments.

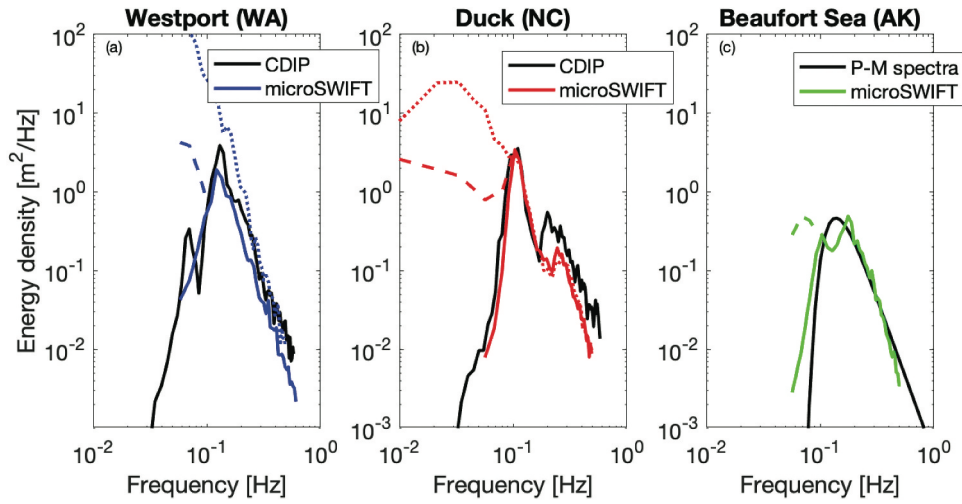| Project | Location | Dates | Method | Groundtruth | $H_s$ range |
|---|---|---|---|---|---|
| Westport testing | WA coast | July 2021 | Vessel | Waverider | $2 - 3$ m |
| DUNEX | Duck FRF | Oct 2021 | Air (helicopter) | Waverider | $1 - 2$ m |
| Arctic coastal ice | Beaufort Sea | Sept 2021 | Air (Twin Otter) | none | $1 - 2$ m |
| NHCI | Gulf of Mexico | Sept 2022 | Air (P3) | Spotter | $1 - 8$ m |

**Figure 6.** Spectra from early testing of microSwifts (v1). The solid colored lines are the GPS-based onboard processing. The dashed lines are the GPS-based result without the high-pass filter. The dotted lines are the IMU-based onboard processing, which were abandoned in the later testing because of insufficient filtering.

v1 microSWIFTs. The microSWIFTs were allow to drift past the moored waverider and were reset once to stay within 500 m of the waverider. Figure 6a shows the spectral agreement between the Waverider and the microSWIFTs. The GPS results are in good agreement, though the filter is clearly essential to that agreement. The IMU results agree at the highest frequencies, but deviate dramatically at the middle and low frequencies. The aforementioned integration error in the IMU spectral results is severe, such that the RC filter is unable to recover a reasonable result.

## 5.2. Duck FRF (North Carolina, USA)

There were extensive v1-1 L microSWIFT deployments during the 2021 DUNEX experiment at the US Army Corps of Engineers Field Research Facility in Duck, NC (USA). The data and IMU post-processing are described in detail in Rainville et al. (2023). These deployments were focused on nearshore dynamics, but buoys drifted offshore on a few occasions that provide opportunistic validation of wave spectra from the onboard GPS processing. Figure 6b shows the spectral comparison of microSWIFT drifting past the Datawell Waverider CDIP 192 on October 26 2021. The GPS results are in good agreement, though again the filter is clearly essential to that agreement. The microSWIFT was 59 km from the waverider, and there are some differences in the secondary wind-wave peak around $f = 0.5$ Hz that are likely related to small scale wind variations and sea breeze along the coast. As in the previous test, the IMU results have severe errors at low frequencies that overwhelm the RC filters.

## 5.3. Beaufort sea (Alaska, USA)

Ongoing aerial deployments in the seasonally ice-covered Beaufort Sea intend to quantify the dissipation of energy by shorefast ice (e.g. Thomson et al. 2021) and calibrate observations from Distributed Acoustic Sensing (DAS) using a seafloor fiber optic cable (Baker and Abbott 2022; Smith et al. 2023). Deployments to-date have focused on the early and late portions of the open-water season, specifically in the months of September 2021, November 2021, , and June 2022. Figure 6c shows spectra from Sept 2021. No other buoys or wave measurments were available as groundtruth, and thus a parametric Pierson-Moskowitz spectra based on observed 10 m/s winds is used for comparison.

## 5.4. Hurricane Ian

Hurricane Ian was a major hurricane (category IV) that made landfall in Florida in Sept 2022. As part of the NOPP Hurricane Coastal Impacts (NHCI) Program, an array of wave buoys was deployed ahead of the storm using a P-3 aircraft operated by the Navy's VXS-1 Scientific Development Squadron. These have been used to understand the saturation of wave slopes under extreme winds (Davis et al. 2023), while also providing an opportunity for full scale validation of the microSWIFTs. These were open-door deployments ahead of the storm. Future deployments will also use the dropsonde tube of NOAA P-3 aircraft flying inside the storm, which can more accurately target the track of the storm in real-time. (This 2 L size microSWIFT was recently certifed for deployment from the NOAA P-3.)
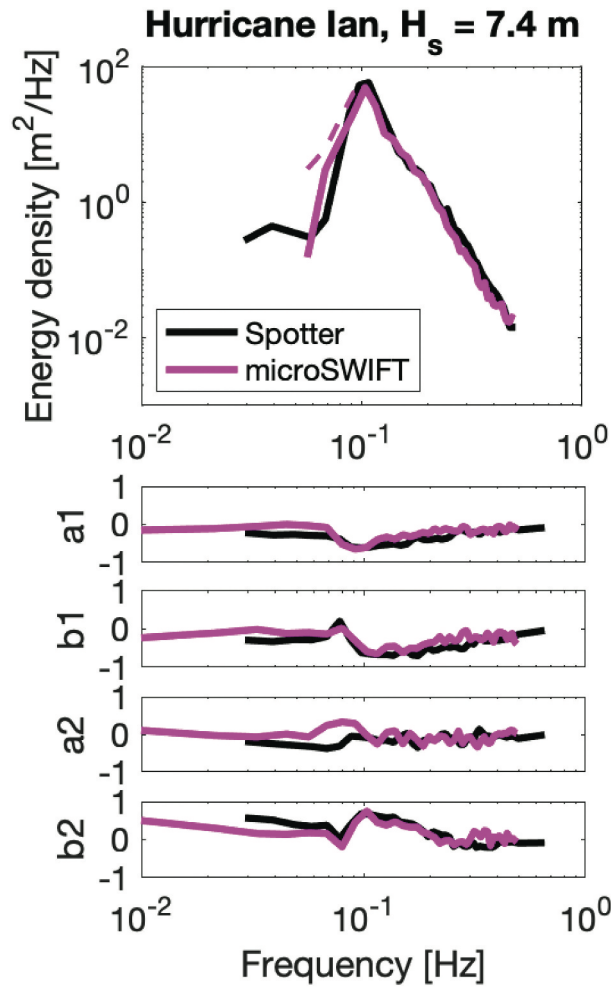
**Hurricane Ian, H_s = 7.4 m**



Figure 7. Spectral results, including directional moments, from a v1 (2L) microSWIFT near a Spotter buoy during Hurricane Ian (Sept 2022). The dashed line is the spectra without a high-pass filter; the solid line includes a high-pass filter. The buoys were 87 km a part during this observation. Spotter data courtesy of Sofar Ocean, Inc.

Spectral comparisons between a microSWIFT and a Spotter are shown in Figures 7 to 9. Each figure has the scalar energy (with and without filtering), along with the normalized directional moments. Figure 7 shows the maximum conditions ($H_s = 7.4$ m) as hurricane passed through the buoy array. Figure 8 shows the energetic conditions ($H_s = 4.3$ m) immediately following the hurricane. Figure 9 shows the calmer conditions ($H_s = 2.7$ m) one day after the hurricane. The agreement between the buoys is strong across all conditions and for all spectral quantities. Quantities derived from these spectra also are in agreement, including full 2-D directional spectra (not shown) that can be reconstructed from the moments $a_1, b_1, a_2, b_2$. The slight differences between buoys at low frequencies has a negligible effect on derived quantities, because the energy levels at those frequencies are so low. These three spectral comparisons are representative of the larger dataset, which includes 68 total observations (i.e. the hourly $H_s$ results in Figure 5).

## 6. Discussion

Though the beta version of the microSWIFT was based on GPS velocity data for wave estimation, the initial design for production versions of the microSWIFTs assumed that IMU data would become the preferred source for wave estimation. This assumption was based on the plethora of low-cost and low-power IMUs now available for consumer electronics. As shown by Rainville et al. (2023), the IMU data collected by microSWIFTs is certainly valuable for resolving the kinematics of individual waves, as well as for detecting the onset and strength of breaking waves. However, such usage requires careful post-processing, with band-pass
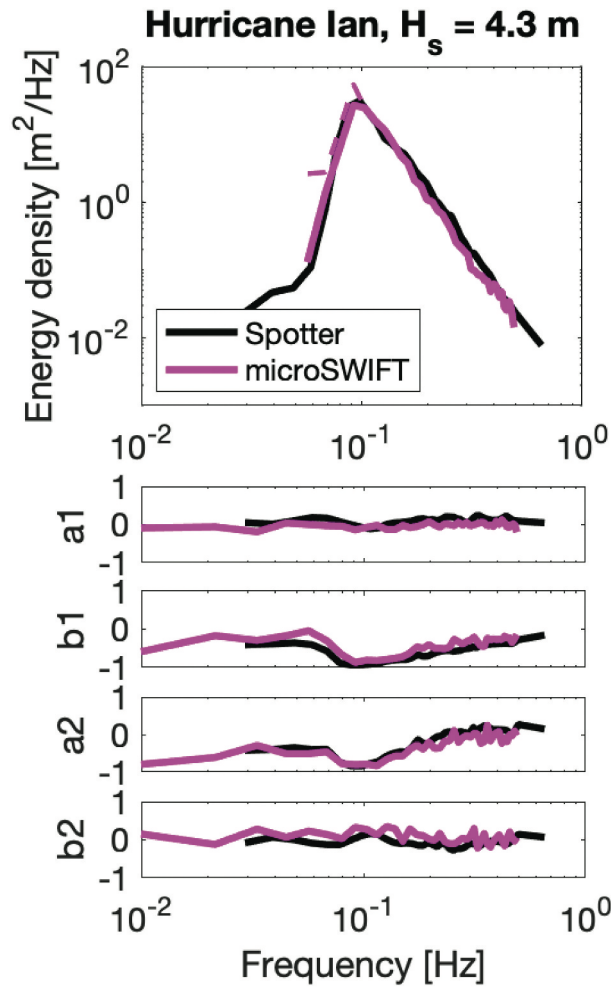
**Figure 8.** Spectral results, including directional moments, from a v1 (2L) microSWIFT near a Spotter buoy immediately following Hurricane Ian (Sept 2022). The dashed line is the spectra without a high-pass filter; the solid line includes a high-pass filter. The buoys were 63 km a part during this observation. Spotter data courtesy of Sofar Ocean, Inc.

filters that are tuned to wave motion and sensor fusion algorithms that include noise characteristics of the linear accelerometers, gyroscopes, and magnetometers. The v1 microSWIFTs included both IMU-based and GPS-based onboard processing, with a flag in the Iridium SBD telemetry packet to identify the data source for each spectral result. As shown in Figure 6, the onboarding processing of IMU data produced results with severe bias at low frequencies.

Use of the IMU data required assuming the vertical axis of the body reference frame was nearly aligned with the vertical axis of the earth reference frame (i.e. a strapped-down accelerometer). This assumption fails in extreme sea states (e.g. hurricanes) and causes large errors in estimation of directional moments $a_1, b_1, a_2, b_2$ from Euler angles (i.e. pitch and roll) in any sea state. Furthermore, the magnetometer readings, which are used to determine heading, require calibration within the buoy housing to remove the effects of additional magnetic fields from batteries and ferrous metals. Based on the difficulties in calibration and tuning of low-cost IMUs, along with the

relatively poor agreement between the IMU onboard processing and the groundtruth measurements, the GPS method is the only onboard processing carried forward into v2.

Even the onboard processing of GPS data required filtering to remove low-frequency noise. This is a persistent problem when using motion data to estimate position. Use of GPS velocities causes a characteristic $f^{-2}$ shape of the noise floor. Use of acceleration would cause $f^{-4}$. Either may by appreciable, relative to the true wave signal, at lower frequencies.

The other surprising aspect of microSWIFT development has been the challenge of working with non-spherical hull shapes. The cylindrical shape used throughout is required for aerial deployments from the drop sonde tube of research aircraft operating at high altitudes with pressurized cabins (i.e. no open-door deployment option). This cylindrical shape makes it difficult to achieve a balance of buoyancy, which is necessary to keep the GPS and Iridium antenna clear, and stability, which is necessary to avoid resonant hydrodynamic response of
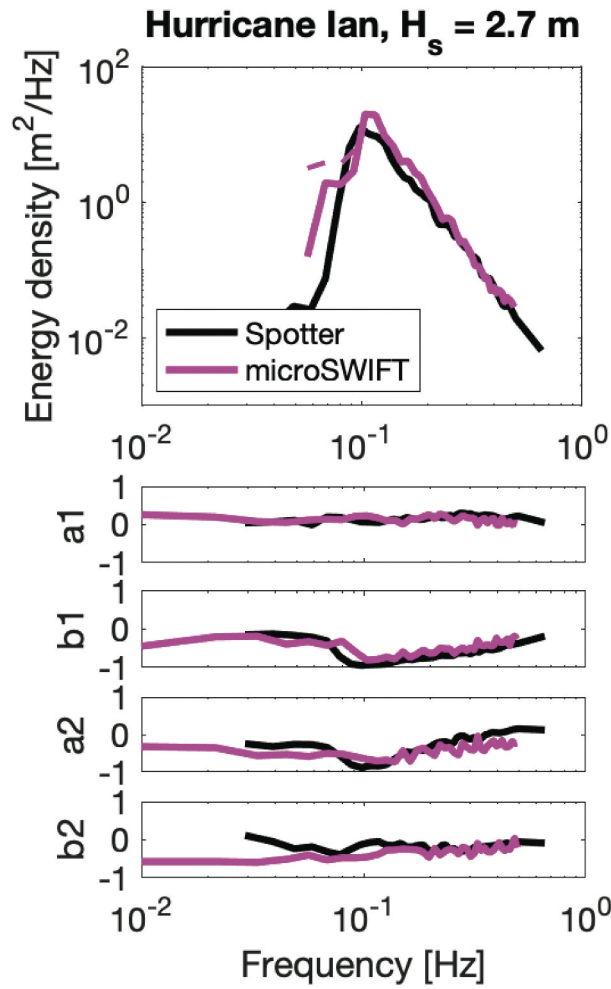
**Figure 9.** Spectral results, including directional moments, from a v1 (2L) microSWIFT near a Spotter buoy one day after Hurricane Ian (Sept 2022). The dashed line is the spectra without a high-pass filter; the solid line includes a high-pass filter. The buoys were 66 km a part during this observation. Spotter data courtesy of Sofar Ocean, Inc.

the buoy. The primary solution has been to add a thin foam octopus collar around the waterline of the microSWIFT hull, which has flexible flaps that fold along the hull when packaged in a cardboard deployment tube. The foam unfolds in the water and provides both additional buoyancy and partial damping of buoy resonance. The secondary solution has been to use GPS velocities as the wave data source because these velocities are agnostic to buoy orientation and are natively in the earth reference frame (not the buoy reference frame).

Following on the favorable comparisons between microSWIFTs and various groundtruth measurements across the field tests, we note that inter-calibration of wave measurements remains a difficult task. As shown by Collins et al. (2024), direct comparisons are often limited by operational constraints, including: mooring dynamics, spectral resolution, buoy endurance, differences in filtering, and differences in parameter definitions. Beyond the practical constraints, there is also the problem of statistical estimates of random waves from

finite records. The convention for wave parameter estimation every 30 or 60 minutes is driven by a requirement for stationarity in the sea state. A 30-minute record might contain over 1,000 realizations for the shorter waves, but only a few hundred realizations for the longer waves. This is enough for robust statistics at all scales since errors in the bulk parameters will reduce with the number of realizations $N$ by a factor $\frac{1}{\sqrt{N}}$, but it can never give the true value that an infinite record will provide. Even small differences in either location or record length will cause non-zero differences in bulk parameters. For the case of buoys drifting independently for several days, such as the Hurricane Ian deployment, the conditions for comparison become far less than ideal.

## 7. Conclusions

The development of miniature, expendable versions of SWIFT buoy has included iterations on processors, housing, and sensors. Each have been

tested to verify sensor noise, hydrodynamic response, spectral fidelity, and aerial survival. Field deployments have spanned a range of environments and wave conditions, including hurricanes and Arctic seas. The microSWIFT buoys are specifically designed for the dropsonde tube of research aircraft, and this opens possibilities for numerous future applications.

## 8. Data and code availability

Telemetry data from all microSWIFTs and SWIFTs are available via public server (see Data tab at www.apl.washington.edu/SWIFT). All associated codes are in repos at https://github.com/SASlabgroup. Specific projects and publications using microSWIFT data have additional archives, such as Dryad https://doi.org/10.5061/dryad.g4f4qrfvb and https://doi.org/10.5061/dryad.hx3ffbgk0.

## ORCID

Jim Thomson 🄳 http://orcid.org/0000-0002-8929-0088
Jacob Davis 🄳 http://orcid.org/0000-0001-8623-2141
Edwin James Rainville 🄳 http://orcid.org/0000-0001-8781-5242

## References

Baker, Michael G., and Robert E. Abbott. 2022. "Rapid Refreezing of a Marginal Ice Zone Across a Seafloor Distributed Acoustic Sensor." *Geophysical Research Letters* 49 (24). https://doi.org/10.1029/2022GL099880. n/a (n/a): e2022GL099880. E2022GL099880 2022GL099880.

Collins, C.O., P. Dickhudt, J. Thomson, T. de Paolo, M. Otero, S. Merrifield, E. Terril, M. Schonau, L. Braasch, T. Paluszkiewicz, and L. Centurioni. "Performance of Moored GPS Wave Buoys." *Journal of Atmospheric and Oceanic Technology*.

Davis, Jacob, Jim Thomson, Isabel A. Houghton, James D. Doyle3, Will Komaromi, Chris W. Fairall, Elizabeth J. Thompson, and J. R. Moskaitis. 2023. "Saturation of Ocean Surface Wave Slopes Observed During Hurricanes." *Geophysical Research Letters* 50 (16). https://doi.org/10.1029/2023GL104139.

Feddersen, F., A. Amador, K. Pick, A. Vizuet, K. Quinn, E. Wolfinger, J. H. MacMahan, et al. 2024. "The Wavedrifter: A Low-Cost IMU-Based Lagrangian Drifter to Measure Surface Gravity Waves from Quasi-Linear to Overturning and the Transition to Turbulence." *Coastal Engineering Journal* 1–14. https://doi.org/10.1080/21664250.2023.2238949.

Herbers, T. H. C., P. F. Jessen, T. T. Janssen, D. B. Colbert, and J. H. MacMahan. 2012. "Observing Ocean Surface Waves with GPS Tracked Buoys." *Journal of Atmospheric and Oceanic Technology* 29 (7): 944–959. https://doi.org/10.1175/JTECH-D-11-00128.1.

Kuik, A. J., G. P. Van Vledder, and L. H. Holthuijsen. 1988. "A Method for the Routine Analyis of Pitch-And-Roll Buoy Wave Data." *Journal of Physical Oceanography* 18 (7): 1020–1034. https://doi.org/10.1175/1520-0485(1988)018<1020:AMFTRA>2.0.CO;2.

Perfect, B., Jim Thomson, Jim Riley, and Endicott Fay. 2015. *Washington State Ferries Rich Passage Wake Study*. Technical Report. Washington State Department of Transportation.

Rabault, Jean, Takehiko Nose, Gaute Hope, Malte Müller, Øyvind Breivik, Joey Voermans, Lars Robert Hole, et al. 2022. "OpenMetbuoy-v2021: An Easy-To-Build, Affordable, Customizable, Open-Source Instrument for Oceanographic Measurements of Drift and Waves in Sea Ice and the Open Ocean." *Geosciences* 12 (3): 3. https://www.mdpi.com/2076-3263/12/3/110.

Rabault, Jean, Graig Sutherland, Olav Gundersen, Atle Jensen, Aleksey Marchenko, and Øyvind Breivik. 2020. "An Open Source, Versatile, Affordable Waves in Ice Instrument for Scientific Measurements in the Polar Regions." *Cold Regions Science and Technology* 170:102955. https://doi.org/10.1016/j.coldregions.2019.102955.

Raghukumar, Kaustubha, Grace Chang, Frank Spada, Craig Jones, Tim Janssen, and Andrew Gans. 2019. "Performance Characteristics of "Spotter," a Newly Developed Real-Time Wave Measurement Buoy." *Journal of Atmospheric and Oceanic Technology* 36 (6): 1127–1141. https://doi.org/10.1175/JTECH-D-18-0151.1.

Rainville, E. J., J. Thomson, M. Moulton, and M. Derakhti. 2023. "Measurements of Nearshore Waves Through Coherent Arrays of Free-Drifting Wave Buoys." *Earth System Science Data*. https://doi.org/10.5194/essd-2023-64.

Smith, M. M., J. Thomson, M. G. Baker, R. Abbott, and J. Davis. 2023. "Observations of Ocean Surface Wave Attenuation in Sea Ice Using Seafloor Cables." *Geophysical Research Letters in revision*. https://doi.org/10.22541/essoar.168889938.88368062/v1.

Thomson, Jim. 2012. "Wave Breaking Dissipation Observed with SWIFT Drifters." *Journal of Atmospheric and Oceanic Technology* 29 (12): 1866–1882. https://doi.org/10.1175/JTECH-D-12-00018.1.

Thomson, Jim, James B. Girton, Rajesh Jha, and Andrew Trapani. 2018. "Measurements of Directional Wave Spectra and Wind Stress from a Wave Glider Autonomous Surface Vehicle." *Journal of Atmospheric and Oceanic Technology* 35 (2): 347–363. https://doi.org/10.1175/JTECH-D-17-0091.1.

Thomson, Jim, Lucia Hošeková, Michael H. Meylan, Alison L Kohout, and Nirnimesh Kumar. 2021. "Spurious Rollover of Wave Attenuation Rates in Sea Ice Caused by Noise in Field Measurements." *Journal of Geophysical Research: Oceans* 126 (3): e2020JC016606. n/a (n/a)E2020JC016606 2020JC016606. https://agupubs.onlinelibrary.wiley.com/doi/abs/10.1029/2020JC016606.

Thomson, Jim, Joe Talbert, Alex de Klerk, Adam Brown, Mike Schwendeman, Jarett Goldsmith, Julie Thomas, Corey Olfe, Grant Cameron, and Christian Meinig. 2015. "Biofouling Effects on the Response of a Wave Measurement Buoy in Deep Water." *Journal of Atmospheric and Oceanic Technology* 32 (6): 1281–1286. https://doi.org/10.1175/JTECH-D-15-0029.1.